Characterization of a landslide geometry using 3D seismic refraction traveltime tomography: The La Valette landslide case history

K. Samyn [a,*], J. Travelletti [b,c], A. Bitri [a], G. Grandjean [a], J.-P. Malet [b]

[a] BRGM, Bureau de recherches géologiques et minières, Orléans, France
[b] Institut de Physique du Globe de Strasbourg, CNRS UMR 7516, Ecole et Observatoire des Sciences de la Terre, Université de Strasbourg, Strasbourg, France
[c] GEOPHEN, LETG, CNRS UMR 6554, Université de Caen Basse-Normandie, Caen, France

ARTICLE INFO

ABSTRACT

The geometry of the bedrock, internal layers and shear surfaces/bands controls the deformation pattern and the mechanisms of landslides. A challenge to progress in the forecast of landslide acceleration in terms of early-warning is therefore to characterize the 3D geometry of the unstable mass at a high level of spatial resolution, both in the horizontal and vertical directions, by integrating information from different surveying techniques. For such characterization, seismic investigations are potentially of a great interest. In the case of complex structures, the measure and the processing of seismic data need to be performed in 3D. The objective of this work is to present the development of a 3D extension of a seismic refraction traveltime tomography technique based on a Simultaneous Iterative Reconstruction Technique (SIRT). First the processing algorithm is detailed and its performance is discussed, and second an application to the La Valette complex landslide is presented. Inversion of first-arrival traveltimes produces a 3D tomogram that underlines the presence of many areas characterized by low P-wave velocity of 500–1800 m.s^{-1}. These low P-wave velocity structures result from the presence of reworked blocks, surficial cracks and in-depth fracture zones. These structures seem to extend to around 25 m in depth over a 80×130 m area. Based on borehole geotechnical data and previous geophysical investigations, an interface corresponding to an internal slip surface can be suspected near the isovalue of 1200 m.s^{-1} at a depth of -10 to -15 m. The stable substratum is characterized by higher values of P-wave velocity of 1800–3000 m.s^{-1}. The features identified in the 3D tomogram allow to better (1) delineate the boundary between the landslide and the surrounding stable slopes, and (2) understand the morphological structures within the landslide at a hectometric scale. The integration of the 3D seismic tomography interpretation to previous geophysical acquisitions using a geostatistical approach allows to construct a 3D geometrical model of the middle and lower part of the La Valette landslide, and to estimate the volume of the unstable mass.

© 2012 Elsevier B.V. All rights reserved.

1. Introduction

Unstable mountain slopes are a serious hazard in populated regions of many countries and may cause important damages and numerous fatalities in mountain and coastal regions (Crozier and Glade, 2005). Rapid population growth observed in mountainous regions coupled with the possible increase of extreme meteorologic events are likely to increase the probability of slope failures (Buma and Dehn, 2003). Comprehensive knowledge of such slopes (e.g. detection and inventory of unstable areas, volumes of the affected slope, displacement monitoring) is a pre-requisite for any quantitative hazard assessment and for the design of effective remediation strategies. More precisely, defining at a high spatial resolution the geometry of the sliding mass and the main structures controlling the mechanism represent a challenge to progress in landslide characterization (Travelletti and Malet, 2012). Landslides have mainly been investigated with standard 2D geophysical techniques (Hack, 2000; Jongmans and Garambois, 2007; McCann and Forster, 1999). For instance, in the last decade, numerous acquisitions of 2D seismic tomography were applied on landslides. They showed that S- and P-wave velocity are parameters of a great interest to characterize intrinsic properties such as the geological layering, the material stiffness or compaction, and the material porosity (presence of fissure; Grandjean et al., 2006; Jongmans et al., 2009). The internal strain affecting soft-rock landslides usually induces a velocity contrast between the unstable mass and the stable bedrock (Caris and van Asch, 1991; Jongmans and Garambois, 2007; Méric et al., 2007). Grandjean et al. (2006) showed that seismic velocities are much more sensitive to the degree of fissuring than the apparent resistivities (acquired through electrical resistivity tomography techniques,

* Corresponding author at: BRGM, Risks Department, 3 Avenue Claude Guillemin BP36009 45060 Orléans Cedex 2, France. Tel.: +33 2 38 64 34 54; fax: +33 2 38 64 36 89.
E-mail address: k.samyn@brgm.fr (K. Samyn).

-ERT) which makes that technique very adapted for structural analyses of landslides.

To progress in seismic imaging technique applied to landslide investigation, a 3D seismic refraction traveltime tomographic techniques has been implemented and tested for the determination of the P-wave velocity field of a specific area in the medium part of the La Valette landslide. The landslide is located in the Ubaye Valley (South French Alps; Fig. 1a) and represents a major risk for the inhabitants (Colas and Locat, 1993). 3D tomographic techniques have already been applied to investigate colluvial wedges along seismically active faults (Morey and Schuster, 1999), fractured reservoirs (Martí et al., 2002), contaminated aquifers (Zelt et al., 2006) and soils of archaeological interest (Polymenakos et al., 2004), and first applications to landslides developed in rock slopes have been proposed (Heincke et al., 2006, 2010).

The objective of this work is to present the development of a 3D extension of the seismic refraction traveltime tomography technique presented by Grandjean and Sage (2004). With the aim of, providing a relevant contribution to a case study, the inversion technique is then applied to characterize the complex geometry and internal structure of the La Valette landslide. First, the main geomorphological features of the landslide are presented. Second, the strategy to acquire the seismic data in the field and the tomographic inversion technique are presented. Third, the interpreted seismic data are discussed and compared to existing knowledge. Important information on the velocity structure within the landslide is provided by the 3D velocity tomogram, as it provides a 3D block pattern of subsurface velocity and details at a high resolution the lateral and vertical extent of the landslide. It reveals an area of low P-wave velocity probably defining a highly fractured zone in depth that correlates with the boundary of the landslide. Finally, the interpretation of the 3D seismic tomography is combined with previous geophysical investigations using a geostatistical approach to propose a 3D geometrical and geological model of the middle and lower part of the landslide, which constitute an incremental step in this case history.

2. The La Valette landslide

2.1. General characteristics

The La Valette landslide, triggered in March 1982, is one of the most important large and complex slope movement in the South French Alps. The landslide affects a hillslope located uphill of the municipality of Saint-Pons in the Barcelonnette basin (Department of Alpes-de-Haute-Provence, France) and is an important threat for around 170 community housings located downstream (Le Mignon and Cojean, 2002).

The La Valette landslide is a case of reactivation of an older landslide (Travelletti et al., 2011) and is characterized with a succession of individual slides as it is often observed in deep-seated landslides (Agliardi et al., 2001). $3.5 \ 10^6 \ m^3$ of material are mobilized over a length of 2 km for a variable width of 0.2 km in the lower and medium parts of the landslide, to 0.5 km in the upper part (Fig. 1a). The mean slope gradient is ca. 30° in the scarp area and ca. 20° in the accumulation area. The maximum thickness varies from 35 m in the upper part (Le Mignon, 2004) to 25 m in the medium and lower parts (Travelletti et al., 2009). For the period 2005–2010, the observed average displacement rate is comprised at 1 to 2 m.year^{-1}.
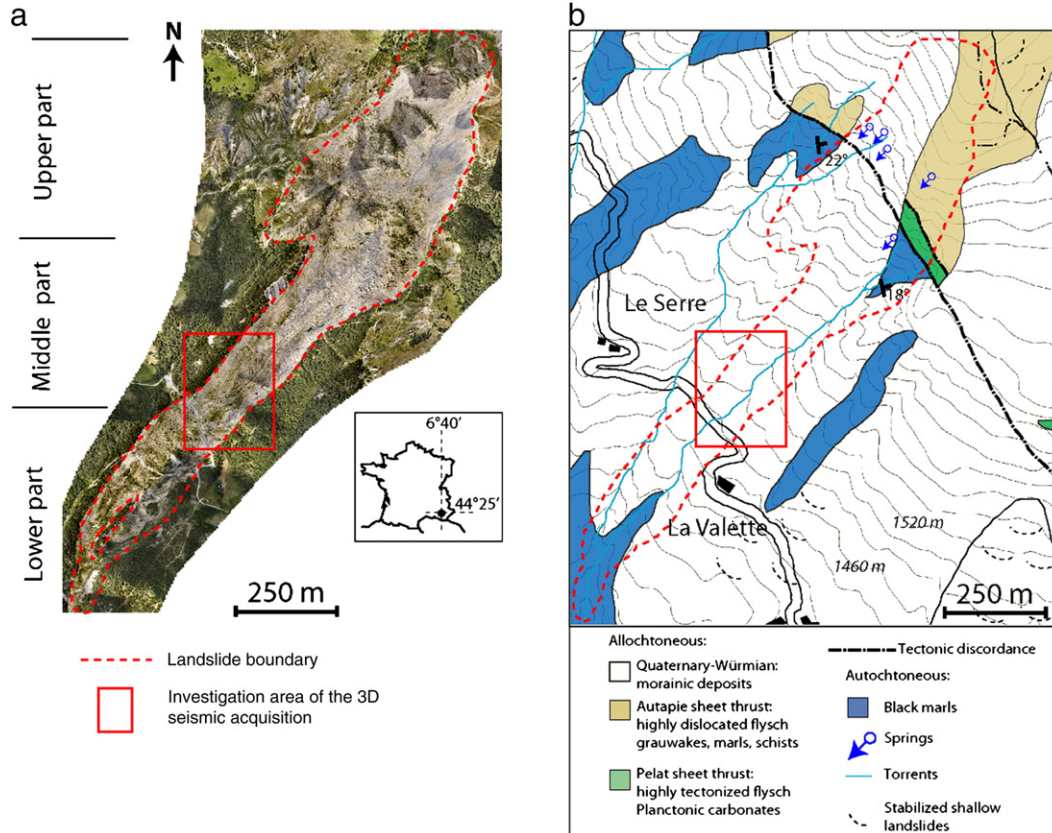
Fig. 1. Geomorphological settings of the La Valette landslide on the South-facing slope of the Barcelonnette basin. (a): orthophotograph of the landslide in 2009, with indication of the studied area in the middle part of the landslide; (b): excerpt of the regional geological map at 1:50,000 scale with the pre-failure topography (before 1982). The torrential gullies are now covered by the unstable mass (adapted from BRGM, 1974).

2.2. Geological and geomorphic settings

From a geological point of view, the La Valette landslide is located at the tectonic contact between two major geological formations outcropping in the tectonic window of the Barcelonnette basin (Fig. 1b):

— An autochtonous formation represented by stratified Callovo-Oxfordian black marls (e.g. "Terres Noires") and characterized by a typical landscape of badlands. This formation is essentially located in the middle and the lower parts of the slope. The bedding plane can easily be identified with a decametric distribution of carbonate discontinuities within the marls;
— An allochtonous formation represented by two nappes in which the upper part of the landslide has developed. The basal nappe is a tectonic wedge belonging to the Pelat nappe and is composed of highly fractured flysch and planctonic carbonates of the Turonian and Paleocene Superior age (BRGM, 1974). This formation has a few dozen of meters of thickness at the location of the main scarp. The Pelat nappe is overlaid by the upper Autapie nappe composed of highly fractured Helminthoid flysch, grauwakes, marls and schist. This formation is dated at the Upper Cretaceous–Upper Eocene (BRGM, 1974).

The tectonic thrust fault between the autochtonous and the allochtonous constitutes a weak zone where many landslide source areas are located in the region (Le Mignon, 2004). This zone is affected by strong weathering processes (mechanical destructuration and weathering due to water circulation in the fractures). These processes lead to a reduction in shear strength of the rock which increases the spatial occurrence of slope failures (Jaboyedoff et al., 2004; Lebourg et al., 2011). Furthermore, the hydrological regime in that part of the landslide facilitates the development of pore water pressures and the saturation of the terrains due to the presence of springs in the vicinity of the tectonic thrust explained by the contrast of permeability between the black marls and the flysch formations (Travelletti et al., 2011).

From a geomorphic point of view, the surface topography of the landslide is extremely rugged with a general slope aspect to the South-West. The area is covered by superficial slope debris (boulders, fine sediments) affected by open cracks and characterized by a low density of vegetation cover.

2.3. Landslide history

According to Hungr et al. (2001) and van Beek and van Asch (1996), the la Valette landslide is considered as a flow-like landslide
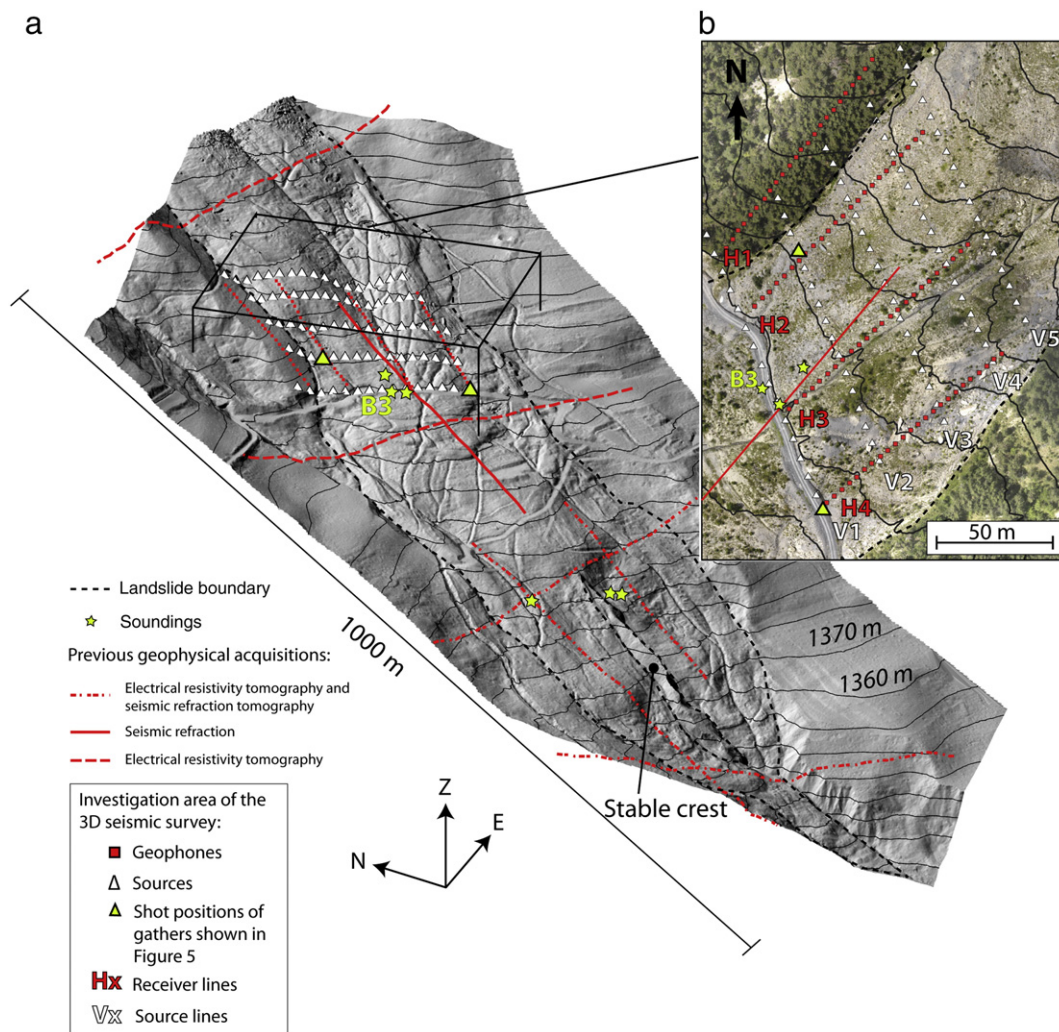
Fig. 2. Location and characteristics of the investigated area within the La Valette landslide. (a): location of all the geophysical and geotechnical data acquired in the middle and lower parts. The black box indicates the location of the 3D seismic survey. The 2D seismic profile is presented in Travelletti et al., 2009 (b): orthophotograph of the investigation area presenting the geometry of the seismic survey. Black triangles and red rectangles show the source and receiver locations, which are arranged along 5 profiles for sources (V1–V5) and 4 profiles for receivers (H1–H4), respectively perpendicular and parallel to the slope. Elevation contours are indicated in meters above sea level.

Table 1
Acquisition parameters used for the 3D seismic survey.

	Line length (m)	Orientation	Source spacing (m)	Geophone spacing (m)	Number of sources	Number of geophones
Geophones lines						
H1	118	SW–NE	30	5	2 inline	24
H2	118	SW–NE	30	5	2 inline	24
H3	118	SW–NE	30	5	2 inline	24
H4	118	SW–NE	30	5	2 inline	24
Total						96
Sources lines						
V1	150	SE-NW	10	50	17	4 inline
V2	150	SE-NW	10	50	16	4 inline
V3	150	SE-NW	10	50	17	4 inline
V4	150	SE-NW	10	50	17	4 inline
V5	150	SE-NW	10	50	18	
Total					85	
Number of traces						8160
Number of picks						8160
Areal extent of the investigation area						118×150 m
Recording system						Geometrics Stratavizor/Geode
Sampling rate						0.5 ms
Source type						Dynamite loads
Charges						100–200 g

characterized by a complex behaviour. The landslide associates two styles of activity: a flow-type behavior with the development of a flow tongue in the medium and lower part and a slide-type behavior with the development of several rotational and planar slides of coherent blocks in the upper part (Fig. 1a, b). Uphill, the slides in the crown area are included in a deeper wedge failure system constrained by pre-existing fractures (Travelletti et al., 2011). The failed mass has progressively loaded the underlying black marls formation, and the landslide has developed by a series of rapid mudflows triggered in the marls such as in March 1982, April 1988, March 1989 and March 1992. The most important acceleration occurred in 1988 when a mudflow of 50,000 m^3 propagated over a runout distance

of ca. 500 m (Colas and Locat, 1993). Up to now, these mudflows did not mobilize the complete failed mass. The consequence of the accumulation of material in the middle and lower parts is an increase in slope gradient and in elevation of the topographic surface. This storage of material is associated to the presence of a stable crest in the lower part that forms a buttress to the progression of the material downhill.

2.4. Previous works

A general presentation and exploratory 1D modelling of the landslide were proposed by Colas and Locat in 1993. In order to decrease the landslide activity, shallow drainage systems were installed in the middle and lower parts of the landslide to impede runoff water to infiltrate. Several benchmarks along profiles were installed in the unstable and stable parts to monitor the displacements using differential single-frequency GPS (Squarzoni et al., 2005). An early-warning system composed of an optical and infra-red camera and debris height detection sensors in the torrent located downstream also are operational since 1991.
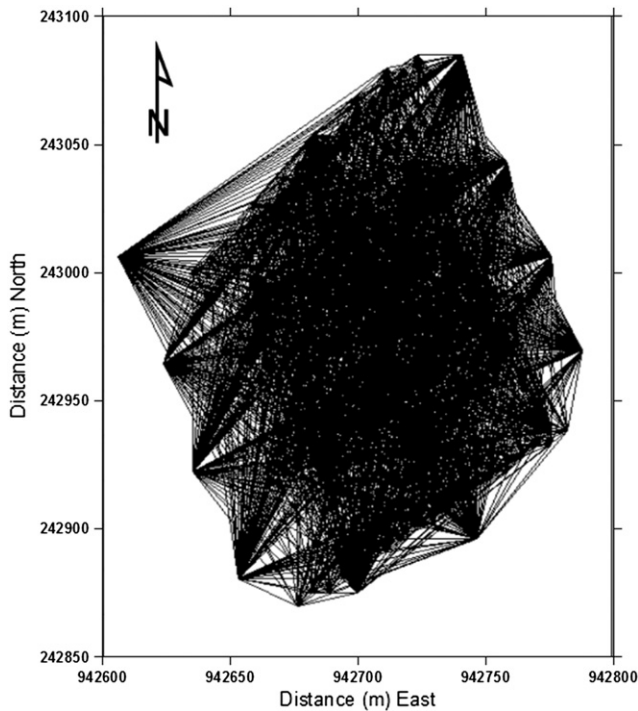
Fig. 3. Representation of the illumination in the entire investigation area obtained by tracing rays between sources and receivers locations. For clarity, only one out of four rays is shown.
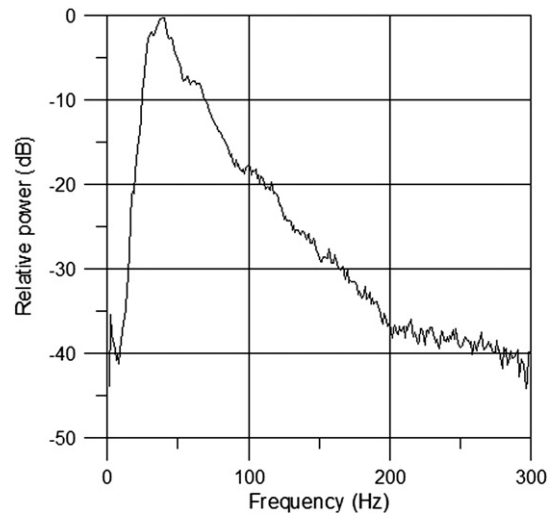
Fig. 4. Frequency spectrum for a typical raw shot gather.
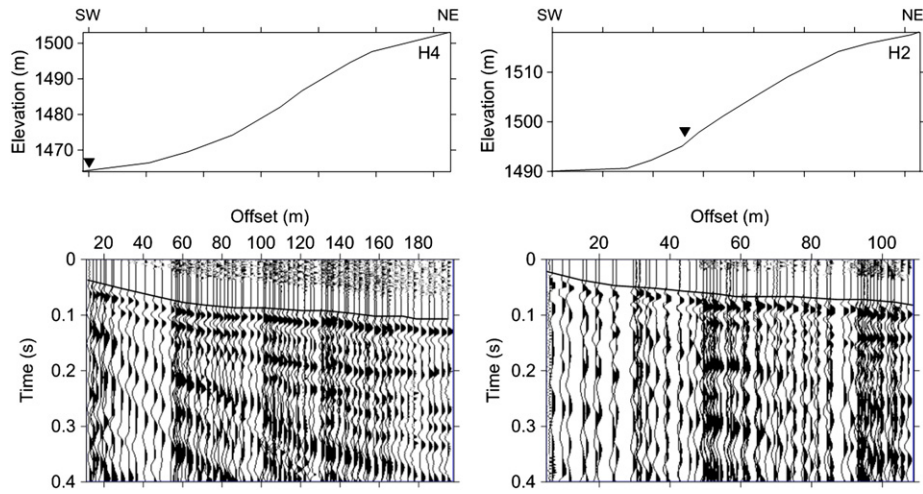
Fig. 5. Examples of selected shot gathers for all the traces of the survey (the location of the selected shots are indicated by a green cross in Fig. 2a,b). Black triangles indicate the shot locations on geophones lines H2 and H4. Black lines show the first-arrival picks. Elevations on the corresponding geophones lines are displayed above the seismic records.

Geophysical (seismic refraction and electrical resistivity tomographies) and geotechnical investigations were undertaken to get an insight of the internal structure to better estimate the volume of the mobilized material. The investigations were mainly concentrated in the upper part (Travelletti et al., 2011) and along the crest in the lower part where the material is accumulated over a maximum thickness of 25 m (Evin, 1992; Travelletti et al., 2009; Fig. 2a). The investigation site is concentrated uphill of the crest at the transition among the middle and lower parts at an elevation comprised between 1465 and 1520 m (Fig. 1a).

3. Characteristics of the data acquisition

The seismic survey was designed to cover both the landslide and a part of the surrounding stable slope (Fig. 2a, b). The layout comprised four 118 m long lines of receivers (H1 to H4) in the downslope direction of the landslide and five 150 m long lines of sources (V1 to V5) perpendicular to the downslope direction of the landslide. Each of the receiver lines corresponds respectively to trace number 1–24, 25–48, 49–72 and 73–96. A destructive geotechnical sounding (B3) equipped with an inclinometer casing) has been realized in 2008
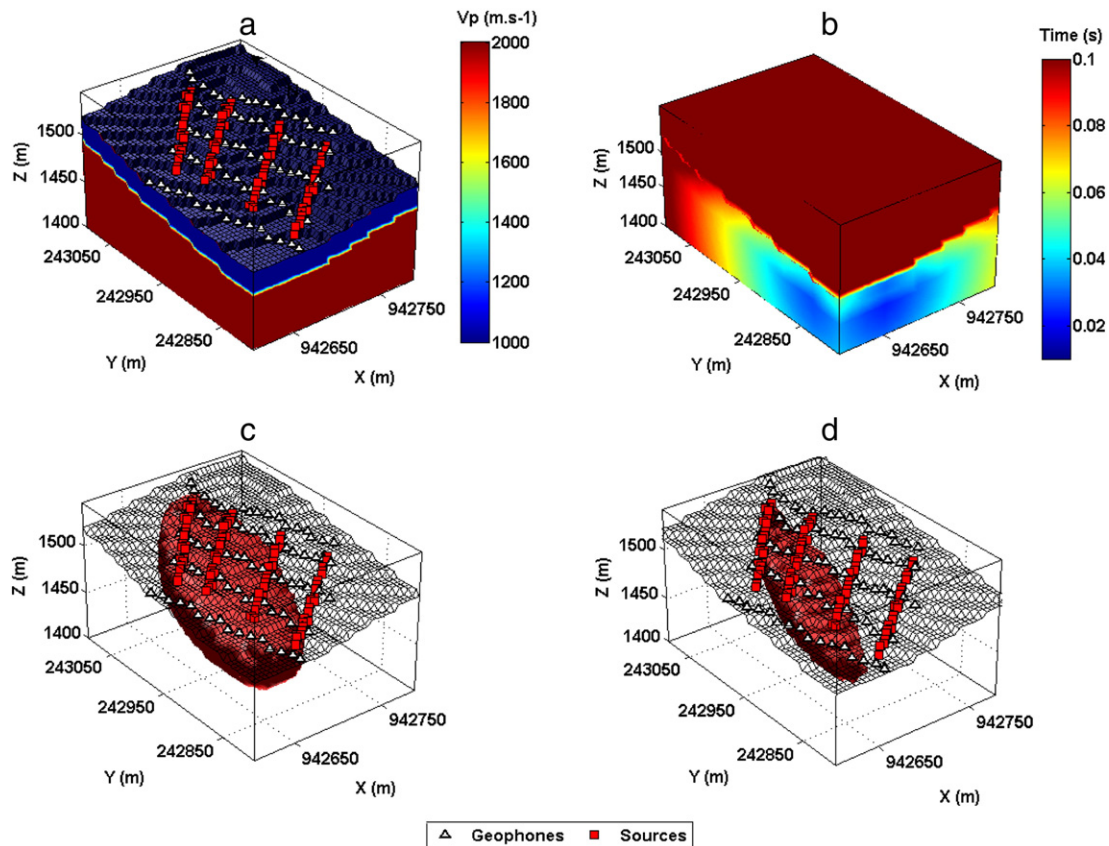
Fig. 6. Synthetic velocity model with the topography used as initial model of the investigation area at the La Valette landslide (a), traveltimes volume (b) and two Fresnel wavepaths computed with frequencies of 50 Hz (c) and 100 Hz (d). Source and receiver for (b), (c) and (d) are, respectively, located at (X = 942650 m, Y = 242850 m, Z = 1455 m) and (X = 942700 m, Y = 2443050 m, Z = 1510 m).

and is located in the lower part of the seismic survey (Fig. 2a, b; Fondasol, 2008). Because of the rapid shearing of the tube at about 15 m in depth, two additional destructive geotechnical soundings were realised at the same place in 2011. Twenty four 10 Hz Mark Products vertical geophones were deployed every 5 m along each receiver line (e.g. a total of 96 geophones for the acquisition) and connected to 24 to 48 channels recording systems from Geometrics. The seismic sources consisted in small shot of dynamite loads of 100–200 g installed every 10 m along each source line in the shallow depth at 0.5–0.7 m drilled auger and crowbar holes according to the terrain state. Acquisition parameters used for the seismic survey are gathered in Table 1 and the acquisition geometry is represented in Fig. 2b.

The signals generated by these shots were recorded by geophones along all the profiles, thus providing a relatively high degree of 3D coverage (Fig. 2b). Together, the uniform areal distribution of sources and receivers over the survey area yielded a good and homogeneous illumination of the subsurface (Fig. 3). Data acquisition was nevertheless complicated by the rugged topography of the terrain with elevations varying in a 10 to 70 m range along the profiles.

The data were recorded using a 0.5 ms sampling rate and contain frequencies ranging from 25 to 200 Hz (Fig. 4). The raw data present a limited dominant frequency of 45 Hz (Fig. 4) due to the use of dynamite loads installed in the very shallow depth and to the frequency filtering behaviour of the landslide reworked material. As indicated on Fig. 5 which presents a selection of typical shots, the data quality can be considered as good to very good in the sense that the high S/N ratio allows a good distinction of first arrivals in the entire offsets range on almost every seismic shot of the data set. Maximum offsets at which first-arrival times were picked reach 205 m. In the selected shot of Fig. 5, the changes in P-wave velocity near the offset 65 m is an argument for significant depth variation in the physical properties of the mass. This change is most likely caused by the presence in depth of a P-wave velocity contrast along the slip surface. From the total of 85 shots, 8160 first-arrival times were picked manually with an accuracy of 1 to 4 ms.
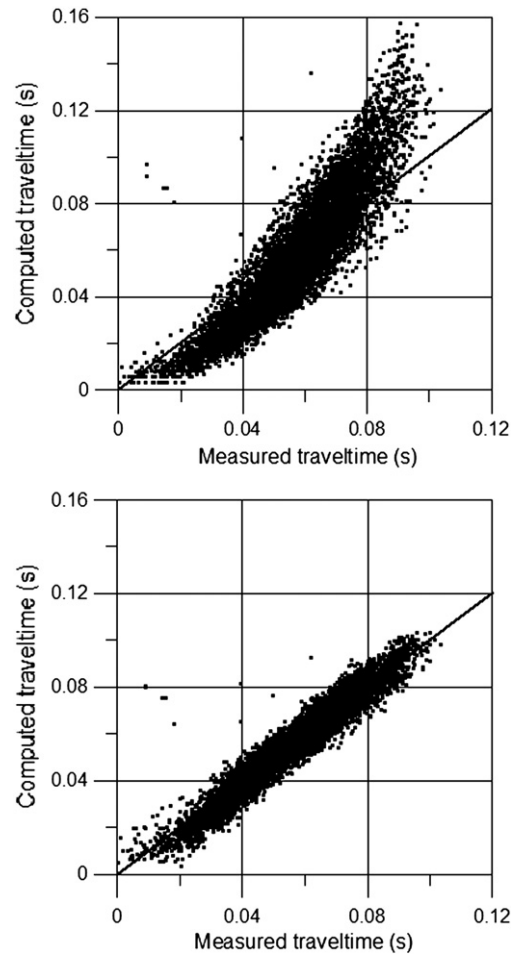
Fig. 8. Comparison between the measured and computed traveltimes for the initial (top) and final (bottom) velocity model. The RMS traveltime misfits for the initial and the final model are, respectively, 11.2 ms and 3.9 ms.
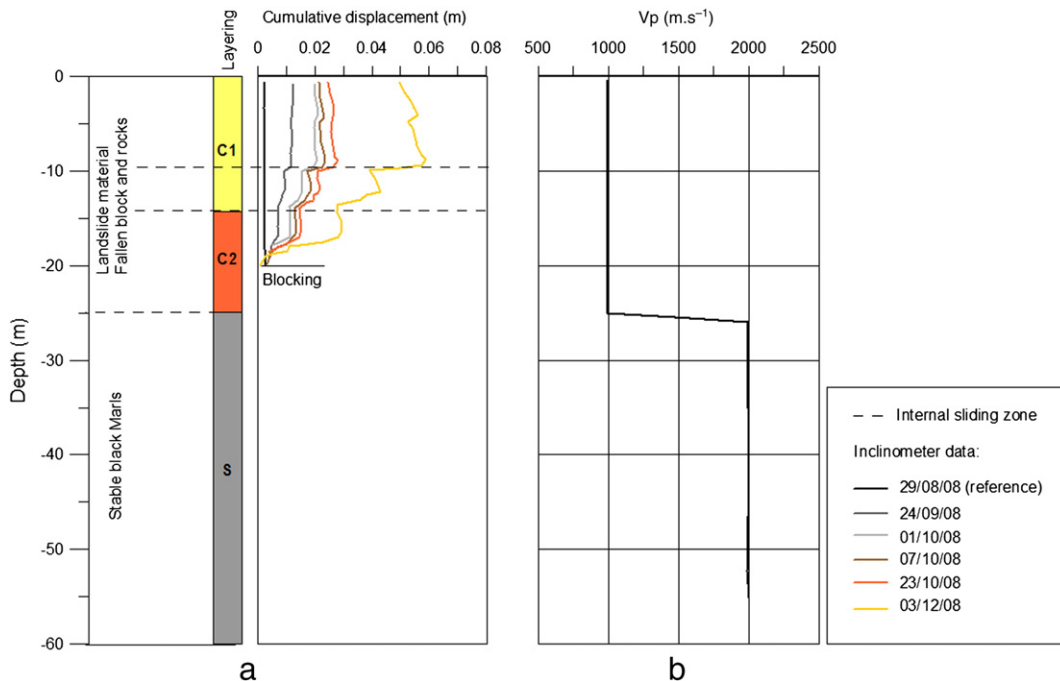
Fig. 7. Vertical structure of the landslide (a): Schematic representation of the material layering and inclinometric observations for which the reference date is 29/08/08 at the borehole B3 (between 0 and 60 m depth; adapted from the geotechnical report by Fondasol, 2008). C1–C2 and S represent the two geotechnical units and the substratum respectively; (b): 1D P-wave velocity model used as starting model. A 3D view of the initial model is also shown in Fig. 6a.
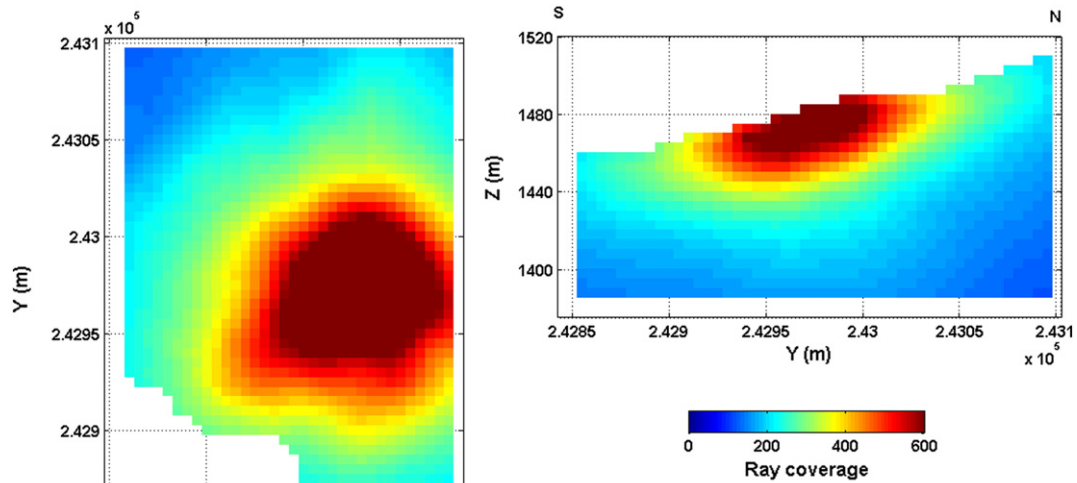
Fig. 9. An example of ray coverage representing the number of Fresnel volume that path through each model cell corresponding to a 1460 m elevation slice (top) and a X = 942690 m north–south cross-section (bottom).

4. Characteristics of the 3D first arrivals traveltime inversion technique

4.1. Presentation of the algorithmic scheme

The program used to invert first arrivals is a 3D extension of the 2D seismic tomography software of Grandjean and Sage (2004). The core program is mainly based on two algorithms, respectively dedicated to the traveltime computation and to the velocity model reconstruction. A second-order Fast Marching Method (FMM) is used to solve the Eikonal equation over a highly discretized numerical grid, therefore enabling a fast and robust computation of seismic traveltimes between sources and receivers. Wavepaths are computed using 3D Fresnel volumes that enter in the regularization strategy and ensure a good convergence. This approach accounts for complex velocity models and has the advantage of considering the effects of the wave frequency in the velocity model resolution (Husen and Kissling, 2001). The velocity model reconstruction is based on a simultaneous iterative reconstruction technique (SIRT).

4.2. The Fresnel wavepath approach

Cerveny and Soares (1992) used a "paraxial ray theory" to define Fresnel volumes. In a medium between source S and receiver R, the Fresnel volume is defined by the set of points P, where the waves are delayed after the shortest traveltime t_{SR} by less than half a period.

Considering the ray approximation, i.e. the infinite spectral bandwidth assumption, the main issue of this approximation lies in the traveltime computation taken as line integrals along the rays spreading over the slowness model. Because the slowness values are only considered along ray paths, the problem is often underdetermined and leads to numerical instability (Baina, 1998). In practice, this difficulty is generally by-passed using regularization operators to reduce the non-constrained part of the model, and then, to reinforce the numerical stability. However, such regularization operators require the selection of appropriate parameters (eigenvalue cutoff and especially the size and weights of the smoothing operators). Husen and Kissling (2001) and Kissling et al. (2001) demonstrated the dependency of these parameters on the resolution and the quality of the final model in poor wavepath coverage areas. This is why the use of a physically-based regularization operator such as Fresnel volumes is preferable since they are based on non-subjective principles completely defined by the problem.

The Fresnel wavepath approach considers the wave frequency in the analysis, thus enabling the evaluation of the tomography resolution and reducing the sparseness of the ray distribution. Frequency band-limited waves propagating in the ground are thus affected not only by structures along the raypath, as assumed by the ray theory, but also by structures located in the vicinity of the ray path. The 3D
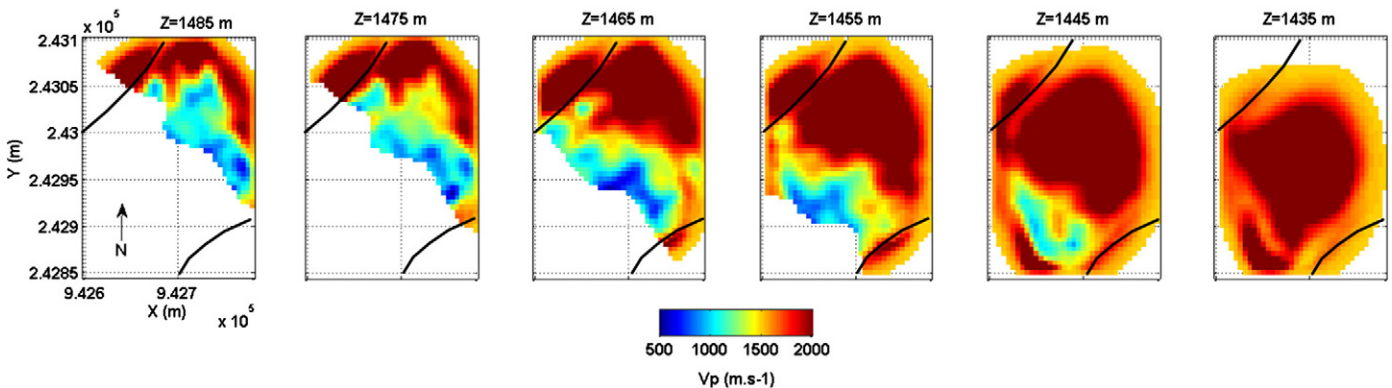
Fig. 10. Spatial distribution of P-wave velocity through the final inverted 3D model at 10 m elevation intervals below the altitude 1500 m. The black solid lines correspond to the landslide boundaries as outlined from geomorphologic observations. Areas which are not sampled by Fresnel volumes appear in white.

formulation of an algorithmic scheme based on Fresnel wavepath could then lead to perform relevant time-saving 3D seismic survey with lower sources and receivers coverage than the one required by the ray path formulation. For our algorithmic scheme, we used a 3D extension of the algorithm for the calculation of Fresnel volumes proposed by Watanabe et al. (1999).

As a demonstration, Fig. 6 shows a representation of a simple synthetic acoustic model with the topography of the investigation area at the La Valette landslide (a) and two Fresnel wavepaths are shown for frequencies of 50 Hz (c) and 100 Hz (d). These examples illustrate how the wave frequency determines the medium affecting the wave propagation.
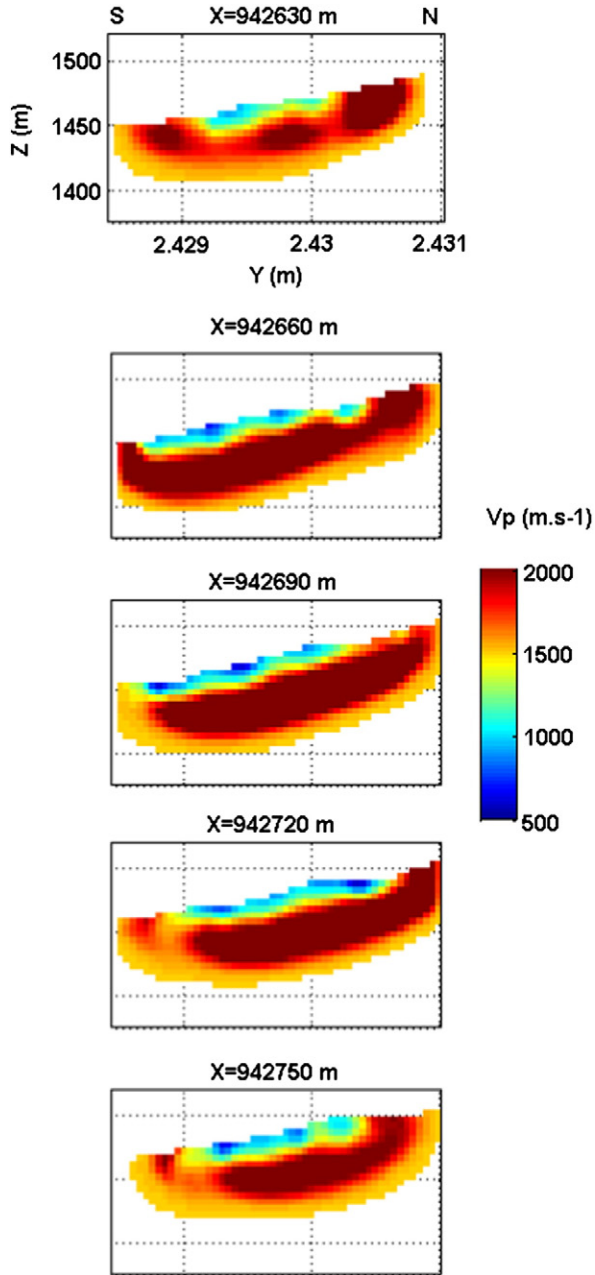
Fig. 11. From top to bottom, north–south P-wave velocity cross-sections through the final inverted 3D model at 30 m distance intervals to the east from the position X = 942630 m. The black dotted lines correspond to the isovalue 1800 m.s^{-1} of P-wave velocity and indicated the sliding contact among the landslide mass and the stable bedrock. Areas which are not sampled by Fresnel volumes appear in white.

4.3. Traveltime calculation

Solving the eikonal equation on a discrete lattice by a fast tracking scheme was presented by Cao and Greenhalgh (1994). In the 3D space, the FMM proposed by Sethian and Popovici (1999) uses an upwind scheme for resolving the following eikonal equation:

$$|\nabla t(x,y,z) = s(x,y,z)| \tag{1}$$

where t is the traveltime field and s is the slowness function. Applying the upwind approximation to the gradient, the computing of the traveltimes in Eq. (1) requires the solution of the equation:

$$\max\left(D_{ijk}^{-x}t,0\right)^2 + \min\left(D_{ijk}^{+x}t,0\right)^2 + \max\left(D_{ijk}^{-y}t,0\right)^2 + \min\left(D_{ijk}^{+y}t,0\right)^2 + \max\left(D_{ijk}^{-z}t,0\right)^2 + \min\left(D_{ijk}^{+z}t,0\right)^2 = s_{ijk}^2 \tag{2}$$

where $D_{ijk}^{-x}t$ can be expressed as a backward x difference operator $(t_{i-1,j,k} - t_{i,j,k}/\Delta x)$ at cell (i, j, k) and S_{ijk} is the slowness at the cell (i, j, k). Numerically, this scheme consists in successively searching to which grid point of the lattice the wavefront has to be propagated. Starting from the source point, tagged FROZEN, we calculate the traveltime at its neighbors. We store these four grid points, tagged BAND, in a heap representing the wavefront. The grid point having the smallest traveltime is then extracted from the heap. We calculate its neighbor's traveltime and push them in the heap. This procedure, which actually mimics a monotonously expanding wavefront, is repeated until the lattice, points tagged FAR, has completely been scanned. Considering the topography, grid points having higher elevation coordinate then the topographic elevation are set to FROZEN so that no traveltime is calculated for those points. Fig. 6b shows a representation of the wavefront function computed with the 3D formulation of the FMM for the synthetic landslide model with the topography shown in Fig. 6a.

4.4. The reconstruction algorithm

The velocity model reconstruction is based on a SIRT, originally described by Dines and Lytle (1979) and reformulated to integrate 3D Fresnel wavepaths by using a probabilistic approach (Grandjean and Sage, 2004). In the 3D space, the updating matrix of slowness S can thus be expressed as:

$$S_j^{k+1} = S_j^k \left(1 + \frac{1}{N}\sum_{i=1}^{N}\frac{\Delta t_i}{t_i^C}\frac{\omega_{ij}}{\sum_{j=1}^{M}\omega_{ij}}\sum_{j=1}^{M}S_j\right), j = (x,y,z). \tag{3}$$

That differs from the Grandjean and Sage (2004) SIRT equation for which $j = (x,z)$. In Eq. (3), indices i,j,k denote respectively the wavepath number, the grid point and the iteration number; N and M refer respectively to the number of wavepaths and to the number of grid points; t_i and t_i^C are respectively the observed and computed traveltimes; ω_{ij} is the Fresnel weight of the wavepath i at the grid point j. The 3D extended SIRT reconstruction algorithm computes the average slowness update value on cell $j = (x,y,z)$. It assumes that every Fresnel wavepath having the same total weight $\sum_{i=1}^{M}\omega_{ij}$ has an equal probability of explaining the Δt between the observed and the calculated traveltimes.

5. Application of the 3D tomography inversion to the La Valette dataset

5.1. Construction of the initial model

The geotechnical model of the investigated area at the La Valette landslide associates (1) a surface layer corresponding to the landslide mass and composed essentially of blocks embedded in a silty–clayey matrix of reworked black marls, and (2) a substratum corresponding to the bedrock of black marls (e.g. "Terres Noires"). The inclinometric observations in the borehole B3 locate the contact among the landslide material and the substratum at a depth of −25 m (Fig. 7a). From previous 2D seismic surveys (Grandjean et al., 2009; Travelletti et al., 2009), the true P-wave velocity field is expected to be highly variable and complex both laterally and vertically, with average values of approximately 1000 and 2000 m.s^{-1} for, respectively, the landslide mass and the substratum (Fig. 2a).

Therefore, an initial 1D model with a 1000 m.s^{-1} velocity layer and a 2000 m.s^{-1} velocity halfspace has been used to start the inversion (Figs. 6a and 7b). For grid cells with higher elevation (Z) coordinates than the topographic elevation, cells were set to FROZEN, meaning that the velocity of these cells will keep the Vp value of the starting model and will not change during the inversion. The 3D SIRT inversion was performed at a mesh size of 5×5×5 m.

5.2. Analysis of the 3D tomographic inverted model

The inverted final model was determined after traveltime tomographic inversion using the initial model. The starting RMS traveltime misfit is 11.2 ms and the misfit provided by the final model after twenty iterations is 3.9 ms (Fig. 8). The results of the inversion indicate that our source–receiver configuration is suitable for delineating large-scale structures from the surface to a depth of 50 m.

Fig. 9 presents an example of ray coverage in the sense of Fresnel zones for a 1460 m elevation slice and a X = 942,690 m north–south cross-section in the final 3D tomogram. Ray coverage is a rough indicator of how well the model is constrained at each point of the mesh grid. Ray coverage is maximum between 0 and 20 m depth, with the deepest rays reaching nearly 55 m. Ray coverage is concentrated toward the eastern side of the model between X values of 942,650 and 942,800 m. To emphasize the resolved regions of the 3D tomogram, areas which are not sampled by Fresnel volumes were masked and appear white on Figs. 10–12. To highlight the most significant variations in velocity, we limit the colorscale to 500–2000 m.s^{-1} for these figures.

Spatial distribution of P-wave velocity at 10 m elevation intervals below the elevation 1485 m are presented in Fig. 10. A low-velocity anomaly dipping roughly in the direction northeast–southwest is identified in each slice and contrasts with edges of higher velocity values (1800–3000 m.s^{-1}). The anomaly reaches its lowest velocity value of around 800 m.s^{-1} at the center of the model for the elevation z = 1465 m and covers almost the full width of the model. Those low velocities likely result from the presence of fallen blocks, cracks, fracture zones and faults on a wide variety of scales in the landslide formation as the shape of the low-velocity anomaly is generally consistent with the lateral boundaries of the landslide.

Fig. 11 shows a series of north–south cross sections at 30 m distance intervals through the final 3D model. The model is generally smooth with a small outcropping dome-like structure almost centered on the position y = 243,000 m and characterized by higher P-wave velocity (1800–3000 m.s^{-1}). The isovelocity surface takes the form of a broad depression, roughly in agreement with the geometry and direction of the sliding surface. This is the prominent northeast–southwest low velocity anomaly seen in Fig. 10. The boundaries of the low-velocity anomaly are characterized by higher velocities (1800–3000 m.s^{-1}) on the north and south edges and are generally consistent with landslide surface boundaries delineated on the aerial ortho-photograph (Fig. 2b). However, lower confidence is given to these edges areas where the ray coverage is lower (Fig. 9). A global 3D view from south-west of the final tomogram and observations are presented in Fig. 12.

The P-wave velocity model is in agreement with isovelocity contours obtained in previous 2D seismic refraction tomography sections (Grandjean et al., 2009; Travelletti et al., 2009). The isovalue of 1200 m.s^{-1} corresponds to the location in depth of an internal slip surface located between 10–15 m depth and identified on the inclinometer data (Fig. 7a-13). Therefore this isovalue may be interpreted as the contact among two internal geotechnical units (C1, C2) of reworked material above the stable substratum (S). The velocity contrast between the unconsolidated landslide mass (C1, C2) and the
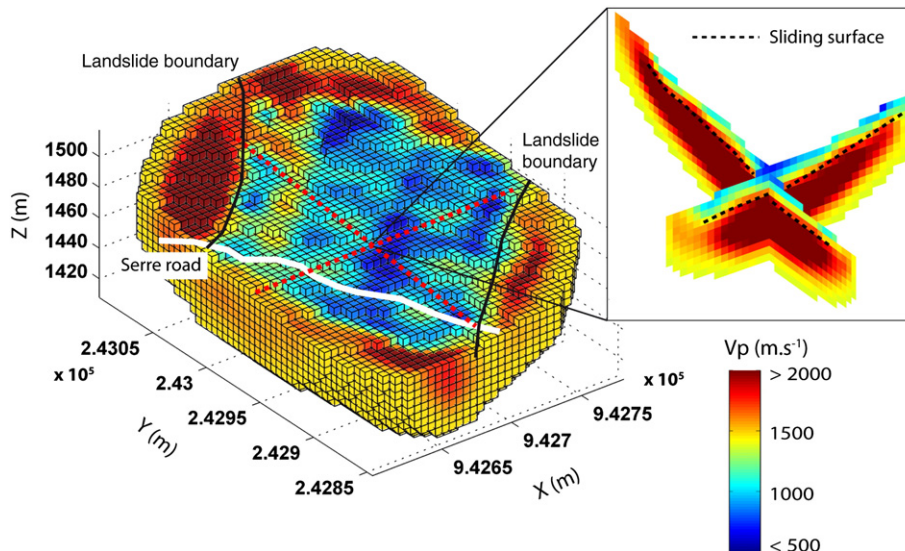
Fig. 12. Global 3D view from south-west of the final tomogram and observations. The black solid lines correspond to the landslide boundaries. The white solid line corresponds to the Serre road crossing the landslide. The red dotted lines correspond to the locations of north–south and east–west cross-sections visible in the maximized window. The black dotted lines correspond to the isovalue 1800 m.s^{-1} of P-wave velocity and indicated the sliding contact among the landslide mass and the stable bedrock.

substratum of black marls (S) allows to locate the sliding contact at the 1800 m.s^{-1} P-wave velocity isovalue (Figs. 7a and 13).

Considering the strong heterogeneity of the landslide mass, it is feasible that the nature of seismic energy changes as it crosses some major features such as intact blocks and highly fissured zones characterized by high porosity values. For example, direct and refracted P-waves absorbed at large open fissures may be multiple scattered and/or replaced at longer distances and at later times by P-waves generated as a result of Rayleigh-wave to P-wave conversions. These effects are not taken into account in the first-arrival traveltime tomography as no abrupt lateral changes in the shot gathers has been observed. It is not possible to account quantitatively for the influence of macroscopic anisotropy and the effects of strong P-wave absorption and multiple scattering. Nevertheless, the general distribution of the low P-wave velocity presented in Figs. 10–12 is likely to be a reasonable first-order approximation of the actual configuration in the subsurface.

5.3. Construction of a 3D geometrical model of the middle and lower part of the landslide

The isocontours of P-wave velocity values 1200 m.s^{-1} and 1800 m.s^{-1} are discretized in 3D data points in order to be integrated with the previous geophysical surveys in a 3D geometrical model (Fig. 13); the discretization allows to define respectively 1165 and 1906 data points for the C1 and C2 units. In the 3D seismic tomography, only the data points located in the central part of the tomography (area delimited by highest ray coverage) are used. In order to be coherent with the landslide geometry observed at the surface, the interpolated interfaces are constrained to pass exactly at the position of the mapped landslide boundary by introducing additional data points along the limits.

A Universal Kriging algorithm is used to interpolate each interface. Kriging interpolation techniques take into account the stochastic
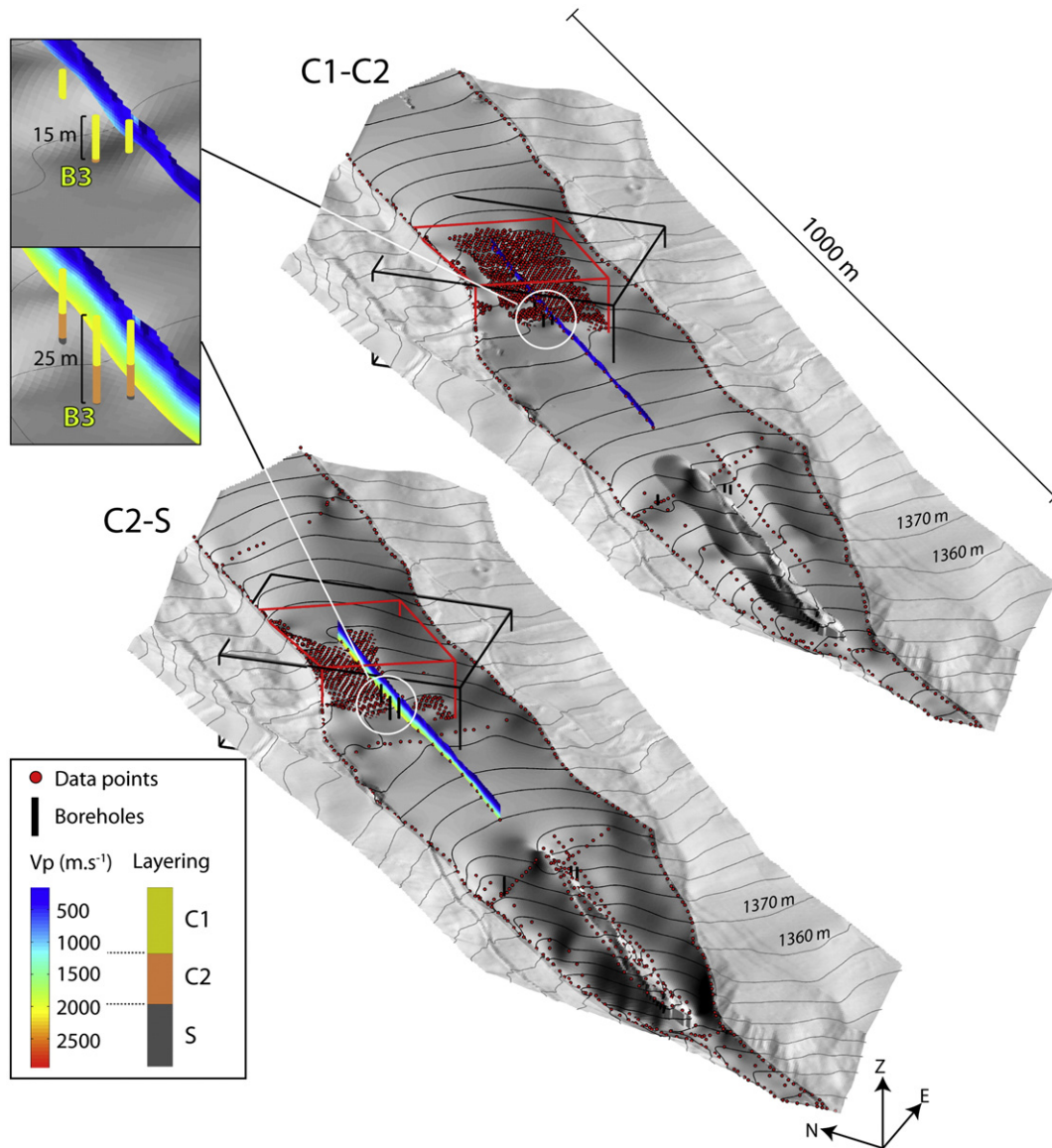
Fig. 13. View of the 3D geometrical model for the interfaces C1–C2 and C2-S interpolated for the middle and lower parts of the landslide. The black box indicates the location of the 3D seismic survey. The red box shows the data points in the center of the 3D seismic survey used for the interpolation of the geometrical model. The geometric model is in good agreement with the layering observed in the soundings and the previous 2D seismic tomography surveys (Grandjean et al., 2009; Travelletti et al., 2009).

dependence among data (which may be the result of a geological process such as sedimentation; Burgess et al., 1981; Marinoni, 2003; Gundogdu and Guney, 2007). This interpolation technique has proven to be very valuable for the interpolation of the geometry of a similar landslide (e.g. Super-Sauze landslide) and for a similar data point distribution (Travelletti and Malet, 2012). Universal Kriging is applied where input data contain a local trend which is, in this study, the mean slope of the investigated area. After removing the trend with a planar regression the semi-variograms are computed on the residual between the trend and the elevation values of the data point. The experimental semi-variogram is modeled with a linear relationship without nugget.

After interpolation of the interfaces in a 5-meter mesh grid, a post-processing is applied to avoid interferences between the interfaces (Caumon et al., 2009; Mallet, 2004; Travelletti and Malet, 2012). Finally, a moving average filter on the gridded interfaces is used to reduce the influence of small-scale variability.

The geometrical model of the middle and lower part of the landslide is presented in Figs. 13–14. The spatial extension of the interface shows the good coherency between the previous 2D seismic survey and the borehole data (Grandjean et al., 2009; Travelletti et al., 2009). Some parts of the model are very well constrained by the data points (e.g. in the 3D seismic survey area) while other parts are more dependent on the interpolation algorithm of the 3D data points derived from the 3D and 2D seismic tomographies and the landslide boundary. The uncertainty on the interface C1–C2 is particularly important since its presence was essentially determined locally in the soundings without inducing a strong contrast in P-wave velocity. The depth of the interfaces varies between 0 and 25 m for the contact C1–C2 and from 0 to 35 m for the contact C2-S (Fig. 14). The geological profiles from the uphill to the downhill part of the landslide highlight the important changes in thickness. The volume of the middle and lower part of the landslide is evaluated at $2.2 \ 10^6 \ m^3$ which represents approximately 60% of the total estimated volume of the landslide.
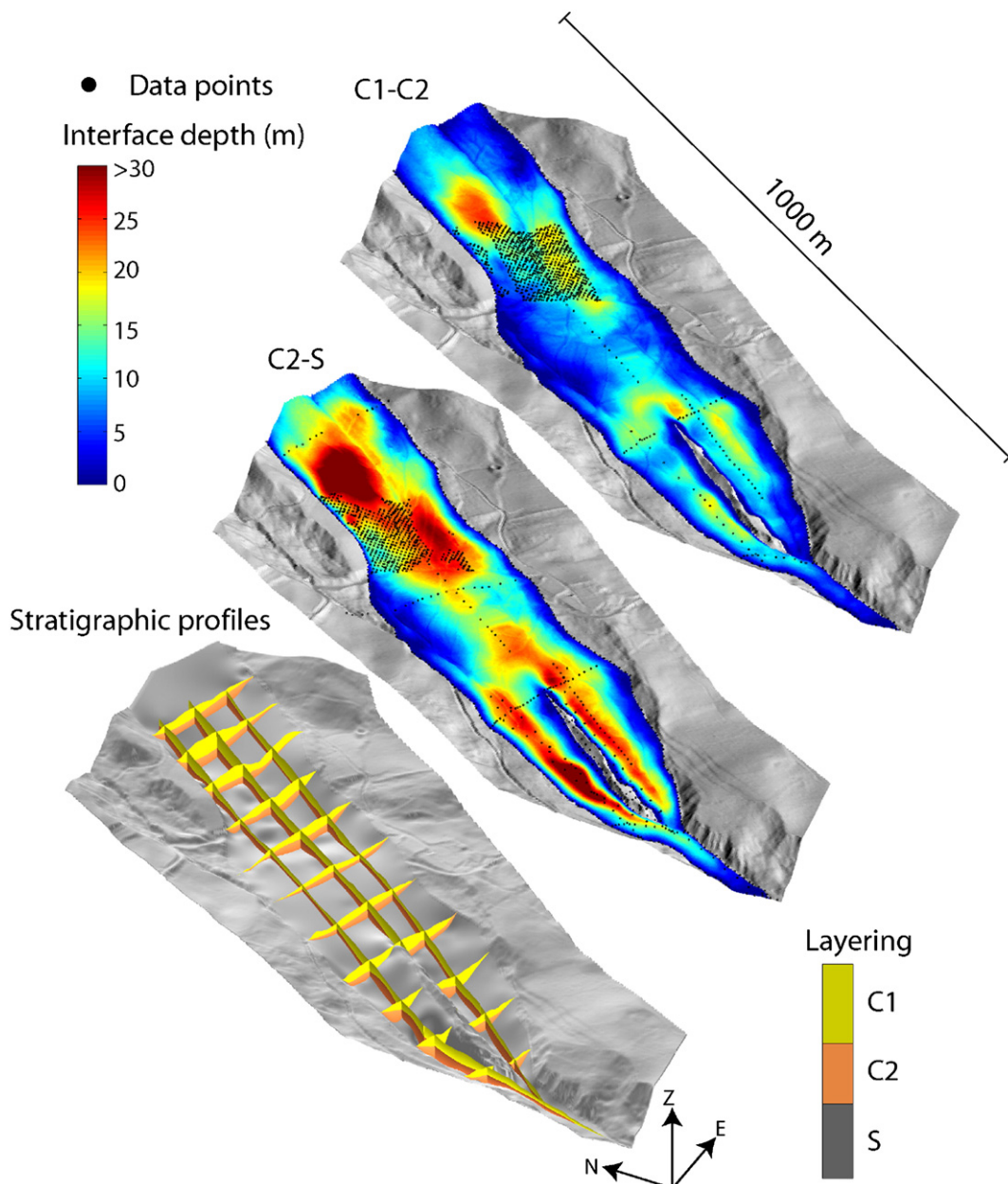
Fig. 14. Maps of the interface depths C1–C2 and C2-S and the corresponding geological profiles.

6. Discussion and conclusion

The algorithms used for traveltime computation are based on a second-order FMM that appears to be fast and accurate enough to compute the Fresnel wavepaths for each source–receiver pair. An extended 3D FMM and SIRT from Grandjean and Sage (2004) are proposed to extract the 3D velocity field. As an application case, we have recorded a 3D seismic data set across an area that includes a part of the unstable mountain slope in the medium part of the La Valette landslide. Let's note that the area described by the seismic survey is limited within the whole extension of the landslide. However, larger 3D seismic survey could easily be achieved in further studies. The study illuminates the 3D seismic structure of the medium part of the La Valette landslide. Inversion of first-arrival traveltimes picked from data recorded on the landslide provided a good fitting between observed and computed traveltimes. The 3D tomogram revealed a broad zone of low seismic velocities that extends inside the visible surface boundaries of the landslide. Low velocities <1800 m.s^{-1} were mapped throughout a volume that extended over a 80×130 m area and a depth of ~25 m (Figs. 10–12). Many surface fracture zones transected the broad low-velocity region. An important part of the investigated volume is probably air-filled void due to the presence of transported blocks. Then, ubiquitous dry cracks, fracture zones, and deconsolidated materials of the landslide were the likely causes of the low velocities. Only in the northeast and southwest edges of the investigation area evidence of stable bedrock formation with velocities around 1800–3000 m.s^{-1} are observed. Estimated P-wave velocities and first order features are in good agreement with previous investigations (borehole and 2D refraction seismic tomography survey). The integration of the 3D seismic tomography interpretation with previous geophysical investigations using a geostatistical approach allows to interpolate an accurate three-layer geological model of the middle and lower part of the landslide. The total volume of landslide material in these parts is evaluated at $2.2 \; 10^6$ m^3. However some areas in the geometrical model are still not very well constrained by data. Moreover, a higher dominant frequency in the data would have provided smaller Fresnel raypaths, which in turn would have justified a closer fit to the data, increasing the model resolution. Therefore the dense spatial resolution supplied by complementary 3D velocity models and the use of higher dominant frequency sources would be very helpful to the extent of the information from the geotechnical and geomorphological analyses. The 3D seismic survey answers the need for providing a valuable and continuous representation of the 3D structure and geology of the landslide.

Acknowledgments

References

Agliardi, F., Crosta, G., Zanchi, A., 2001. Structural constraints on deep-seated slope deformation kinematics. Engineering Geology 59, 83–102.

Baina, R.M.H., 1998. Tomographie sismique entre puits: mise en oeuvre et rôle de l'analyse à posteriori vers une prise en compte de la bande passante. Phd Thesis. Université Rennes 1, France.

BRGM (Bureau des Recherches Géologiques et Minières), 1974. Carte et notice géologique de 651 Barcelonnette au 1:50.000è. XXXV-39. Orléans, France, 38 pp.

Buma, J., Dehn, M., 2003. Impact of climate change on a landslide in South East France, simulated using different GCM scenarios and downscaling methods for local precipitation. Climate Research 15, 69–81.

Burgess, T.M., Webster, R., McBratney, A.B., 1981. Optimal interpolation and isarithmetic mapping of soil properties: sampling strategy. Journal of Soil Science 32, 643–659.

Cao, S., Greenhalgh, S., 1994. Finite-difference solution of the eikonal equation using an efficient, first-arrival, wavefront tracking scheme. Geophysics 59 (4), 632–643.

Caris, J.P.T., van Asch, Th.W.J., 1991. Geophysical, geotechnical and hydrological investigations of a small landslide in the French Alps. Engineering Geology 31 (3–4), 249–276.

Caumon, G., Collon-Drouaillet, P., Carlier, Le, de Veslud, C., Sausse, J., Visuer, S., 2009. Teacher's aide: 3D modeling of geological structures. Mathematical Geosciences 41 (9), 927–945.

Cerveny, V., Soares, J.E.P., 1992. Fresnel volume ray-tracing. Geophysics 57 (7), 902–915.

Colas, G., Locat, J., 1993. Glissement et coulée de La Valette dans les Alpes-de-Haute-Provence. Présentation générale et modélisation de la coulée. Bulletin de Liaison des Laboratoires des Ponts et Chaussées 187, 19–28.

Crozier, M.J., Glade, T., 2005. Landslide hazard and risk: Issues, concepts and approaches. In: Glade, T., Anderson, M., Crozier, M.J. (Eds.), Landslide hazard and risk. John Wiley & Sons, London, pp. 1–40.

Dines, K.A., Lytle, R.J., 1979. Computerized geophysical tomography. Proceedings of the IEEE 67 (7), 1065–1073.

Evin, M., 1992. Prospection sismique en partie basse de la coulée de La Valette. Rapport Interne, RTM Restauration des Terrains en Montagne, Barcelonnette, France. http://eost.u-strasbg.fr/omiv/Publications_la_valette.html.

Fondasol, 2008. Rapport d'étude: Barcelonnette — Glissement de La Valette, Reconnaissances Géotechniques, CCS08010. 30 pp.

Grandjean, G., Sage, S., 2004. JaTS: a fully portable seismic tomography software based on Fresnel wavepaths and a probabilistic reconstruction approach. Computers and Geosciences 30, 925–935.

Grandjean, G., Pennetier, C., Bitri, A., Méric, O., Malet, J.-P., 2006. Caractérisation de la structure interne et de l'état hydrique de glissements argilo-marneux par tomographie géophysique: l'exemple du glissement-coulée de Super-Sauze. Comptes Rendus Géosciences 338 (9), 587–595.

Grandjean, G., Hibert, C., Bitri, A., Travelletti, J., Malet, J.-P., 2009. Geophysical data fusion applied to the characterization of the La Valette landslide. In: Malet, J.-P., Remaître, A., Boogard, T.A. (Eds.), Proceedings of the International Conference on Landslide Processes: from geomorphologic mapping to dynamic modelling, Strasbourg, CERG Editions, pp. 119–124.

Gundogdu, K.S., Guney, I., 2007. Spatial analysis of groundwater levels using universal kriging. Journal of Earth System Sciences 116 (1), 49–55.

Hack, R., 2000. Geophysics for slope stability. Surveys in Geophysics 21, 423–448.

Heincke, B., Maurer, H., Green, A.G., Willenberg, H., Spillmann, T., Burlini, L., 2006. Characterizing an unstable mountain slope using shallow 2D and 3D seismic tomography. Geophysics 71 (6), B241–B256.

Heincke, B., Günther, T., Dalsegg, E., Rønning, J.S., Ganerød, G.V., Elvebakk, H., 2010. Combined three-dimensional electric and seismic tomography study on the Åknes rockslide in western Norway. Journal of Applied Geophysics 70, 292–306.

Hungr, O., Evans, S.G., Bovis, M.J., Hutchinson, J.N., 2001. A review of the classification of landslides of the flow type. Environmental and Engineering Geoscience 7, 221–238.

Husen, S., Kissling, E., 2001. Local earthquake tomography between rays and waves: fast ray tomography. Physics of the Earth and Planetary Interiors 123, 129–149.

Jaboyedoff, M., Baillifard, F., Bardou, E., Girod, F., 2004. The effect of weathering on Alpine rock instability. Quarterly Journal of Engineering Geology and Hydrogeology 37 (2), 95–103.

Jongmans, D., Garambois, S., 2007. Geophysical investigation of landslides: a review. Bulletin de la Societe Geologique de France 178 (2), 101–112.

Jongmans, D., Bièvre, G., Renalier, F., Schwartz, S., Beaurez, N., Orengo, Y., 2009. Investigation of a large landslide in glaciolacustrine clays in the Trièves area (French Alps). Engineering Geology 109, 45–56.

Kissling, E., Husen, S., Haslinger, F., 2001. Model parameterization in seismic tomography: a choice of consequence for the solution quality. Physics of the Earth and Planetary Interiors 123, 89–101.

Le Mignon, G., 2004. Analyse de scénarios de mouvements de versants de type glissement-coulées. Application à la région de Barcelonnette (Alpes-de-Haute-Provence, France). PhD Thesis, Ecole Nationale des Ponts et Chaussées, Paris, France, 210 pp.

Le Mignon, G., Cojean, R., 2002. Rôle de l'eau dans la mobilisation de glissement-coulées (Barcelonnette, France). In: Rybar, J., Stemberk, J., Wagner, P. (Eds.), Landslides, Proceedings of the 1st European Conference on Landslides, Prague, Czech Republik. Swets & Zeiltinger, Lisse, pp. 239–244.

Lebourg, T., Hernandez, M., Jomard, H., El Bedoui, S., Bois, T., Zerathe, S., Tric, E., Vidal, M., 2011. Temporal evolution of weathered cataclastic material in gravitational faults of the La Clapiere deep-seated landslide by mechanical approach. Landslides 8, 241–252.

Mallet, J.-L., 2004. Space–time mathematical framework for sedimentary geology. Mathematical Geology 36 (1), 1–32.

Marinoni, O., 2003. Improving geological models using a combined ordinary-indicator kriging approach. Engineering Geology 69, 37–45.

Martí, D., Carbonell, R., Tryggvason, A., Escuder, J., Pérez-Estaún, A., 2002. Mapping brittle fracture zones in three dimensions: high resolution traveltime seismic tomography in a granitic pluton. Geophysical Journal International 149, 95–105.

McCann, D.M., Forster, A., 1999. Reconnaissance geophysical methods in landslide investigations. Engineering Geology 29, 59–87.

Méric, O., Garambois, S., Cadet, H., Malet, J.-P., Guéguen, P., Jongmans, D., 2007. Seismic noise based methods for soil landslide characterization. Bulletin de la Societe Geologique de France 178 (2), 137–148.

Morey, D., Schuster, G.T., 1999. Palaeoseismicity of the Oquirrh fault, Utah from shallow seismic tomography. Geophysical Journal International 138, 25–35.

Polymenakos, L., Papamarinopoulos, S., Liossis, A., Koukoli-Chryssanthaki, C., 2004. Investigation of a monumental Macedonian tumulus by three-dimensional seismic tomography. Archaeological Prospection 11, 145–158.

Sethian, J.A., Popovici, A.M., 1999. 3-D traveltime computation using the fast marching method. Geophysics 64 (2), 516–523.

Squarzoni, C., Delacourt, C., Allemand, P., 2005. Differential single-frequency GPS monitoring of the La Valette landslide (French Alps). Engineering Geology 79, 215–229.

Travelletti, J., Malet, J.-P., 2012. Characterization of the 3D geometry of flow-like landslides: a methodology based on the integration of multi-source data. Engineering Geology http://dx.doi.org/10.1016/j.enggeo.2011.05.003.

Travelletti, J., Malet, J.-P., Hibert, C., Grandjean, G., 2009. Integration of geomorphological, geophysical and geotechnical data to define the 3D morpho-structure of the La Valette landslide (Ubaye Valley, French Alps). In: Malet, J.-P., Remaître, A., Boogard, T.A. (Eds.), Proceedings of the International Conference on Landslide Processes: from geomorpholgic mapping to dynamic modelling, Strasbourg, CERG Editions, pp. 203–208.

Travelletti, J., Malet, J.-P., Samyn, K., Grandjean, G., Jaboyedoff, M., 2011. Control of landslide retrogression by discontinuities: evidence by the integration of airborne- and ground-based geophysical information. Landslides http://dx.doi.org/10.1007/s10346-011-0310-8.

van Beek, L.P.H., van Asch, Th.W.J., 1996. The mobility characteristics of the La Valette landslide. In: Senneset, K. (Ed.), Proceedings of the 7th International Symposium on Landslides. Trondheim, Norway, Balkema, Rotterdam, pp. 1417–1421.

Watanabe, T., Matsuoka, T., Ashida, Y., 1999. Seismic traveltime tomography using Fresnel volume approach. 69th Proceedings, Society Exploration Geophysics, Houston, USA, SPRO12.5.

Zelt, C.A., Azaria, A., Levander, A., 2006. 3D seismic refraction traveltime tomography at a groundwater contamination site. Geophysics 71 (5), H67–H78.